THE JOURNAL OF BIOLOGICAL CHEMISTRY
Vol. 279, No. 51, Issue of December 17, pp. 53248–53258, 2004
Printed in U.S.A.

Substrate Specificity and Kinetic Mechanism of Mammalian G9a Histone H3 Methyltransferase*

Received for publication, August 20, 2004, and in revised form, October 12, 2004
Published, JBC Papers in Press, October 14, 2004, DOI 10.1074/jbc.M409604200

Debasis Patnaik‡, Hang Gyeong Chin‡, Pierre-Olivier Estève‡, Jack Benner‡, Steven E. Jacobsen§, and Sriharsa Pradhan‡¶

From ‡New England Biolabs, Beverly, Massachusetts 01915, and the §Department of Molecular Cell and Developmental Biology, and Molecular Biology Institute, University of California, Los Angeles, California 90095

Lysine-specific murine histone H3 methyltransferase, G9a, was expressed and purified in a baculovirus expression system. The primary structure of the recombinant enzyme is identical to the native enzyme. Enzymatic activity was favorable at alkaline conditions (>pH 8) and low salt concentration and virtually unchanged between 25 and 42 °C. Purified G9a was used for substrate specificity and steady-state kinetic analysis with peptides representing un- or dimethylated lysine 9 histone H3 tails with native lysine 4 or with lysine 4 changed to alanine (K4AK9). *In vitro* methylation of the H3 tail peptide resulted in trimethylation of Lys-9 and the reaction is processive. The turnover number (k_{cat}) for methylation was 88 and 32 h^{-1} on the wild type and K4AK9 histone H3 tail, respectively. The Michaelis constants for wild type and K4AK9 (K_m^{pep}) were 0.9 and 1.0 μM and for *S*-adenosyl-L-methionine (K_m^{AdoMet}) were 1.8 and 0.6 μM, respectively. Comparable kinetic constants were obtained for recombinant histone H3. The conversion of K4AK9 di- to trimethyl-lysine was 7-fold slower than methyl group addition to unmethylated peptide. Preincubation studies showed that G9a-AdoMet and G9a-peptide complexes are catalytically active. Initial velocity data with peptide and *S*-adenosyl-L-methionine (AdoMet) and product inhibition studies with *S*-adenosyl-L-homocysteine were performed to assess the kinetic mechanism of the reaction. Double reciprocal plots and preincubation studies revealed *S*-adenosyl-L-homocysteine as a competitive inhibitor to AdoMet and mixed inhibitor to peptide. Trimethylated peptides acted as a competitive inhibitor to substrate peptide and mixed inhibitor to AdoMet suggesting a random mechanism in a Bi Bi reaction for recombinant G9a where either substrate can bind first to the enzyme, and either product can release first.

Histones participate in packaging of eukaryotic DNA. Amino-terminal tails of histones are exposed in packed chromatin and are thus amenable to various post-translational modifications. Histone H3 methylation in mammals is implicated in epigenetic gene regulation (1). Other post-translational modifications namely, acetylation and phosphorylation of histone H3 and H4 N-terminal tails are also documented (2, 3). Histone tail modifications are involved in transcriptional activation or repression of chromatin. Generally, acetylated histones mark transcriptionally active chromatin and hypoacetylated chromatin are silent. Furthermore, histone methylation can be a marker for transcriptionally active or inactive segments of the genome (4). Methylation of histone H3 lysine 9 (H3-K9) is a hallmark of silent chromatin and is globally distributed throughout the heterochromatic regions, such as centromeres and telomeres (5). In the inactivated X chromosome of mammals (6) and transcriptionally silent genes in cancer cells frequent H3-K9 methylation is observed (7).

Links between histone methylation and DNA methylation are emerging and have been demonstrated in *Neurospora crassa* and in plants. Experimental evidence have shown that histone methylation as a prerequisite for DNA methylation and transcriptional silencing in *Neurospora* (8) and *Arabidopsis* (9). There are also reports that DNA methylation may trigger H3-K9 methylation in *Arabidopsis* (10, 11), suggesting interplay between histone and DNA methylation in maintaining the silent status of the chromatin. In mammals, H3-K9 directs DNA methylation to the pericentric heterochromatin (12) and to the tumor suppressor gene p16INK4a (13).

Lysine methylation in mammals occurs at the ϵ amino group of the lysine residue. The lysine residues are mono-, di-, or trimethylated. Several histone H3-K9 specific methyltransferases such as Clr4 in yeast (14), Suv39h in mammals, a homologue to *Drosophila* Su(var)3–9 (4, 15), SETDB1/ESET (16, 17), and G9a (18) have been identified. Both Suv39h1 and Suv39h2 play dominant roles in pericentric heterochromatin formation. Both the mouse (Suv39h1 and Suv39h2) and human (SUV39H1 and SUV39H2) genes encode proteins that bind to heterochromatin in association with mammalian HP1. Suv39h1 and Suv39h2 are histone K9-specific methyltransferases and their genetic disruption led to severe reduction in global H3-K9 trimethylation specifically at the pericentric heterochromatic region. Thus it is believed that Suv39h1 and Suv39h2 are responsible for trimethylation of histone H3-K9. The mechanism of Lys-9 methylation of the *Drosophila* Su(var)3–9 enzyme is relatively well studied. Although the methyltransferase domain is required for methyl transfer, mutation at the NH_2 terminus of the enzyme disrupted its *in vivo* functions suggesting co-operation between the NH_2 and COOH terminus for catalysis. This enzyme is a dimer *in vitro* and the NH_2-terminal amino acid residues facilitate dimerization. Disruption of dimerization resulted in 10-fold less enzyme activity, suggesting interaction between the NH_2 and COOH terminus for catalysis (19). The other histone methyltransferase, G9a, is also shown to be involved in Lys-9 methylation of histone H3 on non-heterochromatic loci that are involved with transcriptionally active genes. Genetic disruption of G9a in mouse embryonic stem cells resulted in significant disruption of histone

* This work was supported by New England Biolabs and National Institutes of Health Grant GM60398 (to S. E. J.). The costs of publication of this article were defrayed in part by the payment of page charges. This article must therefore be hereby marked "*advertisement*" in accordance with 18 U.S.C. Section 1734 solely to indicate this fact.

¶ To whom correspondence should be addressed. Tel.: 978-927-5054 (ext. 227); Fax: 978-921-1350; E-mail: pradhan@neb.com.

H3-K9 dimethylation and to a lesser extent H3-K9 monomethylation (20). Loss of G9a also resulted in reduction of H3-K9 methylation in the Prader-Willi syndrome imprinting center resulting in disruption of CpG methylation of the Prader-Willi syndrome imprinting center in mouse ES cells (21). G9a is considerably larger than Suv39h1 and Suv39h2. G9a has a stretch of polyglutamates at its NH_2-terminal region along with characteristic ANK repeats suggesting protein-protein interaction. Like all other histone methyltransferases it has a COOH terminus that contains the SET domain (22). Tachibana *et al.*, (18) have described substrate specificity and sequence specificity of G9a but the reaction mechanism is yet to be elucidated.

In this study an attempt was made to determine lysine 9 methylation events for substrate specificity and kinetic analysis of recombinant murine full-length G9a on a variety of synthetic peptides mimicking the NH_2-terminal tail of histone H3 with an aim to learn about the mechanism of methyl transfer from the co-substrate AdoMet to the peptide. The kinetic parameters for methylation with those peptides and recombinant intact histone H3 substrate are reported herein for full-length G9a. We have also performed initial velocity and product inhibition studies to determine the reaction mechanism of the enzyme.

EXPERIMENTAL PROCEDURES

Histone H3 Methyltransferase G9a Transfer Vector—G9a expression constructs were derived from pZKmG9aL, accession number AB077210 (gift of Prof. Yoichi Shinkai, Kyoto University). This plasmid contains the full-length murine G9a cDNA based on the previously published sequence (18). A PCR of the 3′ end of the cDNA was used to incorporate an EcoRI restriction endonuclease site in place of the stop codon of the cDNA and to provide the optimal amino acids for intein-tag cleavage (sense primer, 5′-CGGGGTACCTCCGGACTGGGGAGGAGCTGGGC-3′ and antisense primer, 5′-GGCCTCGAGGAATTCGGTGTTGATGGGGGGCAGGGAGCT-3′). The restriction sites are underlined. The addition of an EcoRI site resulted in addition of Glu and Phe to the last amino acid Thr of G9a. This PCR product of about 200 bp was digested with BspEI and EcoRI and ligated to LITMUS 28i (New England Biolabs) to give rise to pLitmus 28iG9a3′. The NsiI-BspEI fragment of G9a was excised from mG9aL and cloned into pLitmus 28iG9a3′ to give rise to pLitmus 28iG9aII. This construct contains the entire murine G9a cDNA except for the first ~800 bp. The first 800 bp were PCR amplified (sense primer: 5′-GGCTCGCGAAACATGCGGGGTCTGCCGAGAGGGAGG-3′ and antisense primer: 5′-CCTTCCCCAGATGCATGTCATCAC-3′) and digested with NsiI and cloned into pLitmus 28iG9aII digested with SnaBI and NsiI resulting in a G9a full-length clone, pLitmus G9afl, without a stop codon at the 3′ end along with an NruI site at the 5′ end and an EcoRI site at the 3′ end of the cDNA. The full-length cDNA without the stop codon was excised using NruI and EcoRI and ligated into pVIC1 digested with the same enzymes resulting in pVICG9a (Fig. 1). In pVICG9a the cDNA remained in-frame with the intein chitin-binding domain of transfer vector pVIC1. The ligated junctions in the final pVICG9a construct were verified by DNA sequencing.

Insect Cell Culture, Viral Transfection, and Recombinant G9a Expression—Sf9 cells (Invitrogen) derived from the pupal ovarian tissue of the fall army worm, *Spodoptera frugiperda*, was used for co-transfection and expression of G9a as described previously (23, 24) with the following modifications. Sf9 cells were maintained as a suspension culture in TNM-FH media (JRH Biosciences) supplemented with 10% fetal calf serum (v/v) and an antibiotic-antimycotic solution at a final concentration of 5 units of penicillin, 50 μg of streptomycin, and 0.125 μg of amphotericin B ml^{-1} at 27 °C on a Bellco stirring platform at 70 rpm. Co-transfection of a monolayer of Sf9 insect cells was carried out using BaculoGold DNA, a modified, linearized *Autographa california* nuclear polyhedrosis virus DNA (BD Pharmingen), and the transfer vector pVICG9a. Four days after transfection, the supernatant was amplified 2 to 3 times to reach a viral titer above 2×10^8 ml^{-1} as estimated by the agarose overlay technique (24). Recombinant viruses were used for test expression by infecting 1.5×10^6 Sf9 cells at different multiplicity of infections in a 60-mm Petri dish. Forty-eight hours post-infection, cell extracts were checked for histone H3 methyltransferase activity and for fusion protein expression by Western blot analysis using anti-CBD monoclonal antibody (New England Biolabs). For routine protein expression, Sf9 cells were grown in spinner culture flasks. Sf9 cells at a density of 1.2×10^6 ml^{-1} were infected at a multiplicity of infection between 6 and 10. The cells were kept at 27 °C at 60 rpm and harvested 48-h post-infection after a final wash with 1× phosphate-buffered saline.

Recombinant G9a Purification—For protein purification, infected cells (5.6×10^8) were resuspended in 15 ml of buffer H (50 mM Tris-HCl, pH 8.0, 5 mM $MgCl_2$, protease inhibitor mixture containing 4-(2-aminoethyl)benzenesulfonyl fluoride, pepstatin A, E64, bestatin, leupeptin, and aprotinin (Sigma), 0.2% (v/v) per ml of cell extract, 7 μg/ml phenylmethylsulfonyl fluoride, and 500 mM NaCl). The cell suspension was sonicated on ice for 30 s using a model W-225R (Heatsystem, Ultrasonics) sonicator in pulsed mode at 50% duty cycle. The extract was incubated on ice for 30 min with occasional shaking and centrifuged at $11,000 \times g$ for 30 min. If the supernatant remained cloudy, then one more centrifugation step was included. This supernatant was applied to a chitin bead column (New England Biolabs) equilibrated with buffer H at 0.4 ml/min. Nonspecifically bound proteins were removed by washing with 30 column volumes of buffer H. On column cleavage, the target protein was initiated by passing 2 column volumes of buffer H supplemented with 50 mM dithiothreitol. The column was closed and the target protein was cleaved from the intein-tag by overnight incubation at 4 °C. Recombinant G9a was eluted with buffer H containing 4 mM dithiothreitol and dialyzed against buffer H supplemented with 0.1% (v/v) protease inhibitor mixture (Sigma), 7 μg/ml phenylmethylsulfonyl fluoride, 100 mM NaCl, 50% glycerol (v/v), and 4 mM dithiothreitol. The purified protein was stored at −20 °C. The purity of the protein was checked by SDS-PAGE (4–20% Tris glycine-SDS gradient gel) and quantitated using the Bradford assay with bovine serum albumin as standard.

Histone Methyltransferase Assay—Methyltransferase assays were carried out at 25 °C for 3 min in duplicate with a total volume of 25 μl of reaction mixture. A typical reaction contained *S*-adenosyl-L-[*methyl*-^{3}H]methionine (AdoMet)[1] (specific activity 15 Ci/mmol, Amersham Biosciences), substrate peptide, and enzyme in assay buffer (50 mM Tris-HCl, pH 9.0, 5 mM $MgCl_2$, 4 mM dithiothreitol, 7 μg/ml phenylmethylsulfonyl fluoride). For kinetic analysis, the Lys-9 concentration was calculated from the molecular weight of the substrate peptide. For double-reciprocal plots, the concentrations of peptide and AdoMet were varied. The methyltransferase reactions were stopped by transferring the reaction tubes to an ethanol-dry ice bath or spotted directly on P81 paper circles (Whatman). From each reaction mixture, 10 μl was spotted in duplicate on P81 circles. These circles were washed sequentially three times (5 ml/circle) with cold 0.2 M ammonium bicarbonate and dried. 2.5 ml of SafeScint scintillation mixture (American Bioanalytical) was added to each and tritium incorporation was measured. All methylation values were corrected for nonspecific binding of *S*-adenosyl-L-[*methyl*-^{3}H]methionine to the processed filter. Background calculations were measured in the absence of enzyme at zero time. To calculate counting efficiency, internal tritium standards were used. The efficiency of [^{3}H]DNA measurement was ~55% and all calculations were corrected accordingly. Data obtained were plotted by regression analysis using the GraphPad PRISM 4b program (GraphPad Software Inc.).

To determine the sequence specificity of G9a methylation, 740 nM G9afl enzyme with 192 μM synthetic peptide substrate (K4AK9) and 1.0 mM AdoMet was added in a total reaction volume of 300 μl. At 0, 15-, 30-, 60-, and 120-min intervals, 50 μl of the samples were withdrawn and 5 μl of trifluoroacetic acid was added to stop the reaction. For completion of methylation the last sample was incubated overnight. All reactions were performed at 25 °C.

Analysis of Peptide Methylation by Mass Spectroscopy and Peptide Sequencing—The K4AK9 peptide, CARTAQTARKSTGGY(K-ϵ-biotin), or K4AK9-trimethylated peptide were prepared in-house using Fmoc (*N*-(9-fluorenyl)methoxycarbonyl) chemistry. The peptides were spotted on a 1 mm × 4-mm piece of polyvinylidene difluoride membrane (Problott, Applied Biosystems Inc.) and sequenced using Procise 494 (Applied Biosystems Inc.) according to the procedure of Matsudaira (25), with modifications as described previously (26). The modified H3-(K4AK9-trimethyl) peptide was also sequenced in the same way. The modification of the G9 peptide was also monitored by matrix-assisted laser desorption/ionization time-of-flight (MALDI-TOF) mass spectrometry. The samples were prepared by mixing 1 μl of sample and 3,5-dimethoxy-4-hydroxycinnamic acid matrix dissolved in 50:50 acetonitrile: water contaning 0.1% trifluoroacetic acid and air drying. The spectra

[1] The abbreviations used are: AdoMet, *S*-adenosyl-L-methionine; AdoHcy, *S*-adenosyl-L-homocysteine; MALDI-TOF, matrix-assisted laser desorption/ionization time-of-flight.

were obtained on an Applied Biosystems Voyager DE MALDI-TOF MS instrument.

Peptide Substrates for Methylation Analysis—All peptides were synthesized at New England Biolabs, purified by high performance liquid chromatography, and intactness and purity were checked with mass spectroscopy. Peptides used in this study are listed in Table I. For kinetic analysis all peptides were dissolved in Milli-Q sterilized water and kept frozen at −20 °C before use.

Processivity Studies—A master mixture (600 μl) containing 1.1 μM biotin-conjugated histone H3 tail peptide (Wt-H3), 25 nM G9a, 5 μM AdoMet was incubated at room temperature for 3 min. After 3 min, 300 μl was removed and mixed with 22 μM Wt-H3-nonbiotin tail peptide (no biotin). Aliquots of 25 μl were withdrawn at 3-min intervals up to 15 min, and the reaction was stopped with 1 μl of trifluoroacetic acid. To the reaction mixture 50 μl of 1× phosphate-buffered saline and 25 μl of streptavidin magnetic beads (0.1 mg) were added. The captured peptides were washed with 3× 1 ml of cold 0.2 M ammonium bicarbonate, air dried, and finally dissolved in 100 μl of 0.2 M ammonium bicarbonate and transferred to scintillation vials. 3 ml of SafeScint scintillation mixture was added and mixed before radioactive measurement.

Preincubation Studies—Preincubation experiments were carried out by incubating 25 nM G9a with either 5 μM *S*-adenosyl-L-[*methyl*-^{3}H]methionine or 4.4 μM K4AK9 for 10 min. The reaction was started by adding the missing reactant, *i.e.* peptide (final concentration 4.4 μM) in the first reaction mixture and *S*-adenosyl-L-[*methyl*-^{3}H]methionine (5 μM) to the second one. Aliquots of 10 μl were withdrawn at each minute interval up to 12 min, and spotted directly on P81 and processed as described before.

Enzyme Assay for Initial Velocities in the Absence or Presence of Products and Data Analysis—All initial velocity studies were performed under identical conditions as described for the histone H3 methyltransferase assay. For initial velocity studies with wild type, K4AK9, and K4AK9-dime, the peptides (0.14–4.4 μM) were incubated with 25 nM recombinant G9a and 5 μM *S*-adenosyl-L-[*methyl*-^{3}H]methionine. Product formation was kept below 5% of the substrate. The product formed was measured in counts/min. The nanomolar product formed ([^{3}H]CH_3 group transfer) (N) present at the end of the reaction was calculated as $n = (Y - B)/E \times F$, where Y is counts/min for each experiment, B is counts/min blank, E is efficiency (0.55), F is counts/min/nM free AdoMet. Product formed per min was obtained as N/T, where T is the time of reaction. The nM/min was fitted into a one-site binding (hyperbola) equation as follows.

$$\text{Hyperbola, } v = V_{max}[S]/K_m + [S] \qquad \text{(Eq. 1)}$$

This describes binding of a substrate/ligand to an enzyme that follows the law of mass action. V_{max} is the maximal velocity and K_m is the concentration of substrate to reach half-maximal velocity. All data points were analyzed by nonlinear regression. From V_{max}, turnover number (k_{cat}) was calculated as: $k_{cat} = V_{max}/[Et]$, where $[Et]$ defines total enzyme concentration. For double reciprocal plots, the initial velocity $1/v$ was obtained as $Et \times T/N$. Data points were collected in duplicate, plotted on Lineweaver-Burk double reciprocal plots, and fitted to weighted linear regression. The families of linear regression plots give a preliminary clue toward the nature of the reaction mechanism. These plots essentially gave two independent variables, namely the reciprocals of the apparent V_{max} ($V_{max(app)}$), given by the y axis intercepts and the ratio of the Michaelis constant (K_m) (plus the dissociation constant) for the variable substrate to $V_{max(app)}$, given by the slope. By replotting the intercepts and slopes obtained, one would also determine the true V_{max} and K_m for a substrate. The equations used for fitting the data points and to obtain the kinetic constants, V_{max}, K_m^{pep}, K_m^{H3}, K_m^{AdoMet}, are reported elsewhere (27). These figures represent estimated values.

Initial velocity studies in the presence of products were performed to distinguish the reaction mechanism. G9a has two products at the end of the reaction, one AdoHcy (*S*-adenosyl-L-homocysteine) and trimethylated histone H3 or peptides mimicking the histone H3 tail. AdoHcy (Sigma) was dissolved in 10 N HCl and diluted with Milli-Q water to 100 μM. Methylated peptide was dissolved in Milli-Q water. Assays were performed as described earlier with the exception of addition of a fixed amount of end products. In the experiments with AdoHcy the concentration range of the reactants was 0.14–4.4 μM K4AK9, 0.3–3.0 μM AdoMet, and 0–10 μM AdoHcy. For the assay with trimethylated peptide, the concentration of the reactants were in the range of 0.14–4.4 μM for K4AK9, 0–2.7 μM for K4AK9-trime, and 0.3–3 μM for AdoMet. The sequence of the trimethylated peptide was: CARTKQTAR(tri-meK)STGGKAPRKQLATKAAR(tri-meK)SAPA.

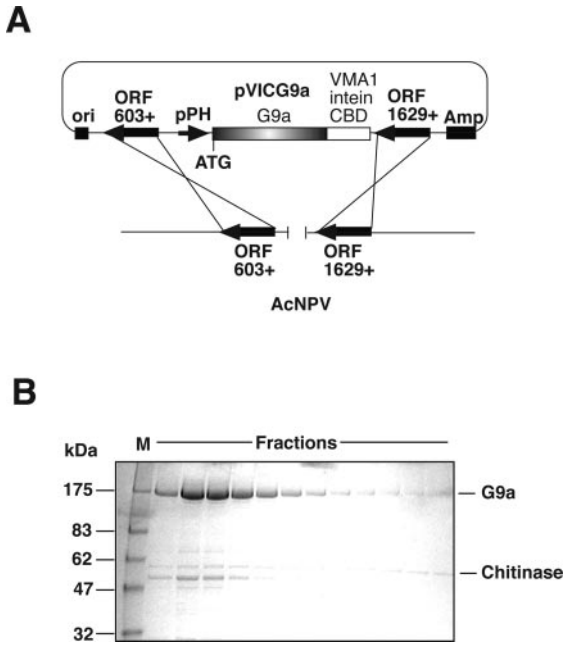

FIG. 1. **Expression and purification of recombinant G9a in a baculovirus expression system.** *A*, diagram representing the murine long isoform G9a construct and its method of integration into the *A. california* nuclear polyhedrosis virus (*AcNPV*) genome. The pVICG9a is shown schematically. A ~3.8-kbp cDNA containing murine G9a, shown in *gray* is fused in-frame with the Sce VMA1 intein-chitin binding domain (*CBD*). A polyhedrin promoter (*pPH*) is situated at the 5′ end of the cDNA upstream of the translation start ATG site. The polyhedrin promoter and G9a cDNA is flanked by viral recombination sequence open reading frames (*ORF*) 603+ and ORF1229+. A recombination event between transfer plasmid pVICG9a and the *A. california* nuclear polyhedrosis virus genome is facilitated by corresponding open reading sequences as shown by the *intersected lines*. *B*, single column purification of recombinant murine G9a. Eluted protein samples from a chitin column were separated on SDS-PAGE and visualized by Coomassie staining. *M* is prestained molecular weight marker from New England Biolabs. The mass of each band is indicated. The co-eluted host cellular chitinase is also shown.

RESULTS

Expression and Purification of Recombinant Histone H3 Methyltransferase G9a—Co-transfection of pVICG9a transfer vector (Fig. 1*A*) with linear *A. california* nuclear polyhedrosis virus DNA (BaculoGold DNA, BD Pharmingen) resulted in homologous recombination of the polyhedrin promoter and the downstream G9a cDNA. Only the recombinant viruses were viable and were amplified further to produce recombinant enzyme in Sf9 cells. A multiplicity of infection of 8 for 48 h, incubation at 27 °C, was found to be optimal for protein expression. The recombinant G9a was soluble and was purified to >90% purity (Fig. 1*B*). The apparent molecular mass of the purified recombinant G9a was about 165 kDa as reported earlier (18). The purified G9a protein was sequenced and had an intact amino terminus (data not shown). A secondary band appeared in this purification that is the host cellular chitinase because of its affinity to the chitin matrix. The dialyzed proteins were stored at −20 °C for several weeks with no apparent loss of activity. We also examined if this residual chitinase presence can have any affect on the methylation reaction in the absence of histone substrates by incubating the enzyme preparation with radioactive AdoMet. A time course of reaction revealed no detectable amount of methylation in the purified fraction (data not shown).

Recombinant proteins were assayed for substrate specificity, optimal pH, and temperature. Methyl transfer was highly dependent on the reaction conditions. At pH 7 the enzyme displayed poor catalytic activity. The velocity of the reaction in-

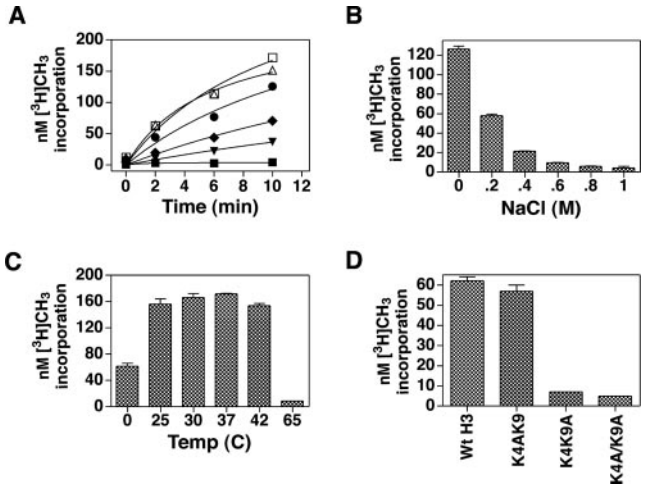

FIG. 2. **Reaction condition optimization for recombinant G9a.** *A*, velocity of the histone methylation reaction with recombinant full-length G9a at various pH values. Methyl group incorporation at pH 7 (*filled square*), 7.8 (*filled inverted triangle*), 8.0 (*filled diamond*), 8.5 (*filled circle*), 9.0 (*open square*), and pH 9.5 (*open triangle*) is shown. *B*, effect of NaCl on histone H3 methylation catalyzed by recombinant G9a. The final NaCl concentration in the reaction is indicated at the *bottom*. *C*, effect of temperature on histone H3 methylation catalyzed by recombinant G9a. Incubation temperature of the reaction is indicated at the *bottom*. *D*, peptides used as substrate for recombinant G9a methylation studies. Peptides are indicated *below* and methylation on the *y* axis. Peptides used as substrate are listed in Table I. All of the above reactions are performed in duplicate with full-length baculovirus-expressed G9a.

creased gradually from pH 7.4 to 9 and dropped slowly after that (Fig. 2A). At pH 11 the enzyme activity dropped drastically (data not shown). The enzyme activity was significantly reduced in the presence of salt (Fig. 2*B*). Remarkably, the recombinant enzyme was capable of methyl group transfer at 0 °C and had no apparent increase in methylation between 25 and 42 °C (Fig. 2*C*). Incubation of recombinant G9a with wild type histone H3 tail peptide or peptide with K4A (K4AK9) resulted in methylation. However, mutation in K9A abolished methyl group incorporation, suggesting that the Lys-9 residue is the target amino acid for catalysis (Fig. 2*D*).

Lysine Trimethylation Is Catalyzed by Recombinant G9a—The ϵ amino group of lysine residues are prone to methylation, with a total possible addition of three methyl groups. Because recombinant G9a histone methyltransferase was able to methylate the histone H3 tail peptide, we synthesized the first 14 amino acids of the NH_2-terminal tail region with a K4A. Therefore, this peptide has only one lysine at position Lys-9 that could possibly be methylated. Furthermore, a chemically synthesized K4A/K9A (Fig. 2*D*) or K4AK9-trimethylated peptide incubated with recombinant G9a did not result in any methyl group transfer (data not shown) confirming that the G9a substrate specificity in the peptide is the Lys-9 residue.

To determine the sequence of methylation events with regard to the number of methyl groups transferred, MALDI-TOF mass spectroscopy was used on *in vitro* methylated synthetic peptides at different time intervals (0, 15, 30, 60, and 120 min and overnight) with cold AdoMet substrate. The molecular mass of the peptide molecule was 2038 daltons. Because one methyl group is 14 daltons, a mono-, di-, or trimethylation will add 14, 28, or 42 daltons onto the peptide substrate if enzymatic methylation occurs. Recombinant G9a was able to methylate the synthetic peptide in a time-dependent manner transferring one methyl group at a time until all available lysine residues were monomethylated (molecular mass 2052). Once the peptides were converted to the mono-Lys-9 methyl peptides, a second methyl group was added until it was converted to di-methyl (molecular mass 2066). Prolonged incubation (overnight) of the enzyme with the substrate converted di-methylated to trimethylated peptide (molecular mass 2080, Fig. 3, *A–E*). These kinetic data suggested that G9a is efficient in mono-, di-, or trimethylation of the Lys-9 residue of the histone H3 tail. Smaller amounts of di- and trimethylated products observed at 15 min of reaction may be because of slow reactivity of the enzyme. To confirm the di- and trimethylation reaction of G9a on synthetic peptide, *in vitro* mock methylated (reaction without enzyme) or methylated (reaction with enzyme) or a control trimethylated peptide substrate was sequenced and the chromatography analysis was compared. In sequencing cycle 10 the mock methylated peptide displayed a peak corresponding to phenylthiohydantoin-lysine (Fig. 3*F*). The presence of lysine at elution cycle 10 is because of addition of a cysteine residue at the amino terminus of K4AK9 thus making the lysine 9 residue the 10^{th} residue in the sequencing reaction. The G9a-methylated K4AK9 peptide (Fig. 3*G*) or K4AK9-trimethylated synthetic peptide (data not shown) produced identical sequences, except that no phenylthiohydantoin-Lys residue was present in cycle 10 but a broad peak that eluted at the same retention time as Tyr was observed. The elution characteristics of this phenylthiohydantoin peak correspond to the previously observed trimethyl-Lys (K-trimethyl) phenylthiohydantoin-derivative (28). These data demonstrate that the overnight reaction converted all di-methyl-lysine 9 to tri-methylated lysine 9 confirming that G9a is capable of trimethylation of the lysine residue of histone H3.

Processivity of Recombinant G9a on Peptide Substrate—To distinguish processive Lys-9 methylation from repeated hit methylation by G9a, the methylation reaction was initiated with the Wt-H3 peptide (biotin tagged) in the presence of a limiting enzyme and excess AdoMet. Three min of preincubation facilitated loading of the AdoMet-G9a complex onto the substrate peptide and performed partial methylation of the substrate as observed in Fig. 4. Following addition of 20-fold excess of Wt-H3-non-biotin peptide, no decrease in methylation on Wt-H3 peptides that were captured with streptavidin magnetic beads was observed. The methylation profile remained almost identical either in the presence or absence of competitor non-biotin substrate (Fig. 4). A repeated hit-methylating enzyme would require dissociating from the substrate after each cycle of methylation. If such a scenario occurs, the dissociated enzyme would have associated with Wt-H3-non-biotin peptide for methylation and resulted in a decrease in methylation on Wt-H3 peptides because streptavidin magnetic beads will not be able to capture non-biotin peptide. Thus, recombinant G9a is a processive enzyme.

Linearity of Methylation Reaction by Recombinant G9a—A time course of methylation using peptide substrate K4AK9 was monitored in the presence of both AdoMet and recombinant G9a to determine the linearity of product formation with time. The reactions were carried out in the presence of either 0.5 or 5.0 μM tritiated AdoMet and a fixed amount of enzyme and K4AK9. In both concentrations the reaction remained linear up to 10 min (Fig. 5*A*). The rate of reaction slowed down after that time possibly because of the formation of AdoHcy. Another set of experiments was performed to determine the concentration of the enzyme at which the rate of product formation remained linear. An increasing concentration of recombinant G9a was added to the reaction mixture containing a fixed amount of K4AK9 and AdoMet. The reaction was allowed to proceed for 3 min and product formation was measured. The reaction essentially remained linear up to an enzyme concentration of 30 nM in the reaction (Fig. 5*B*). Thus the optimal enzyme concentrations in subsequent reactions were established as 25 nM with a 3-min reaction time.

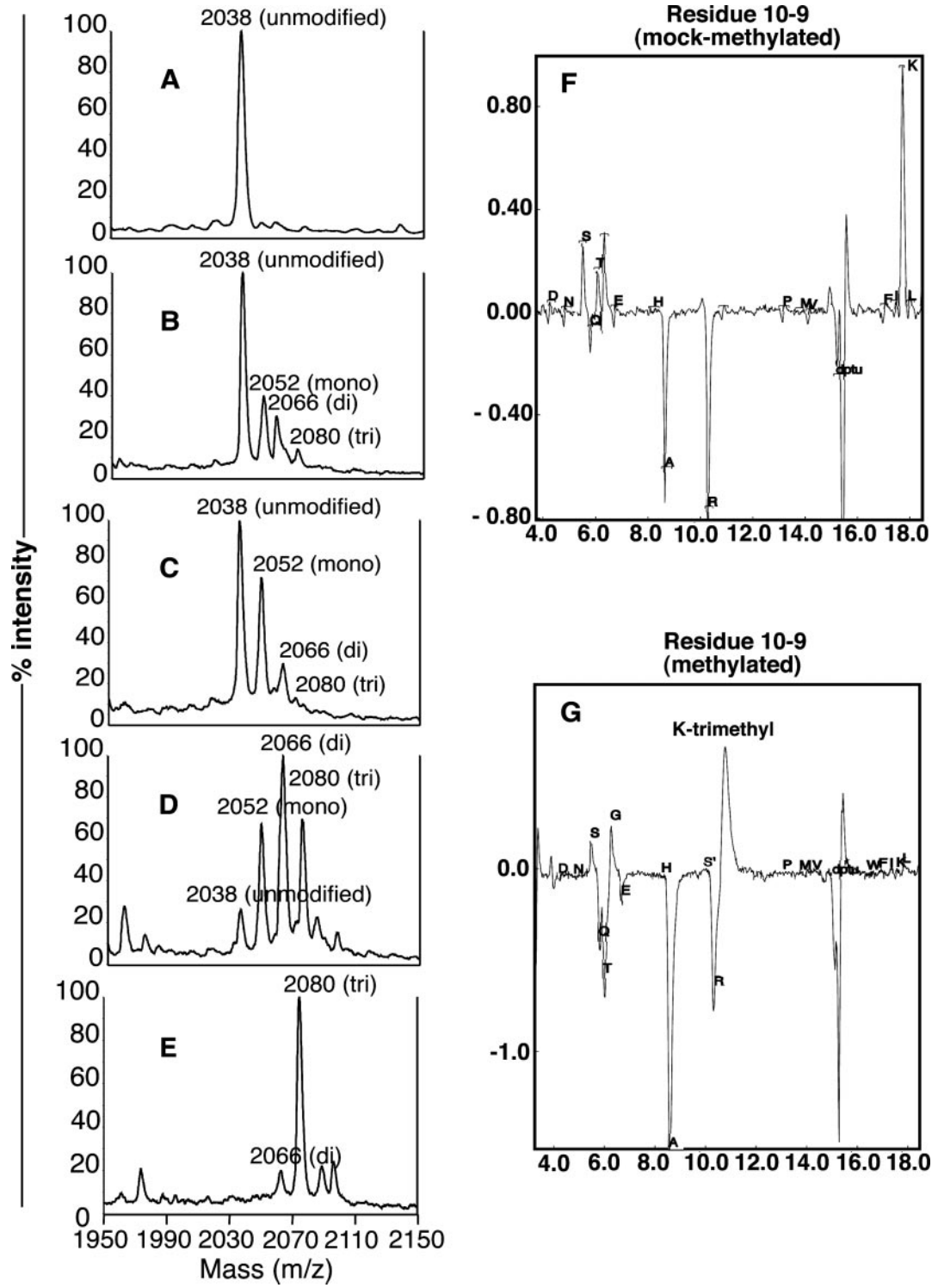

FIG. 3. **Substrate specificity of recombinant G9a.** Mass spectroscopic determination of methylation reaction progression by recombinant full-length G9a (*panels A–E*). Spectras were taken at time 0 (*A*), 15 min (*B*), 30 min (*C*), 120 min (*D*), and overnight (1*E*). Percent intensity is shown at the *left* and mass (*m/z*) on the *bottom*. The incorporation of 1, 2, or 3 methyl groups is indicated as *mono*, *di*, and *tri*, respectively. The molecular masses of unmodified (2038 dalton) mono (2052 daltons), di (2066 daltons), and tri (2080 daltons) are indicated. *F*, the panel shows the high performance liquid chromatogram for cycle 10 of the protein sequencing reaction for mock methylated samples. The large peak corresponding to lysine 9 of the NH_2-terminal tail of histone H3 is visible at the *right* of the chromatogram. *G*, complete trimethylation of lysine by recombinant full-length G9a. The corresponding peak for unmodified lysine (compared with *F*) is very small in the methylated sample in the *right panel*. The trimethyl-lysine peak is predominant in the chromatogram as shown.

Preincubation Studies with Recombinant G9a—G9a is a bisubstrate enzyme. For the catalytic cycle of G9a, binding of the substrates may occur in a random or ordered fashion. To understand the preliminary events of enzyme substrate association and catalytic competency of the binary complexes, recombinant G9a was preincubated with AdoMet or K4AK9 for 10 min and the reaction was initiated with addition of K4AK9 or AdoMet, respectively. Saturating conditions of both AdoMet and K4AK9 and the order of addition of the substrates appear to have a significant influence on the presteady-state methyl-

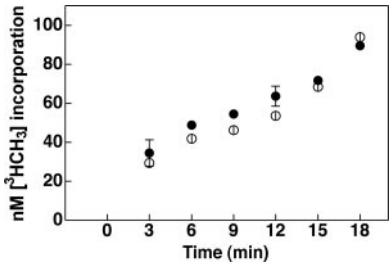

FIG. 4. **Processive methylation catalyzed by recombinant G9a.** Methyl group incorporation after the enzyme was preincubated at 25 °C with tritiated AdoMet and the reaction started by addition of Wt-H3 peptide (*filled circle*). Three min after the start of the reaction the mixture was divided into two sets and one set was chased with Wt-H3-nonbiotinylated excess peptide (*filled circle*) or allowed to proceed without chase (*open circle*), as described under "Experimental Procedures." The reaction was monitored at 3-min time intervals by processing 25 μl of the reaction mixture in duplicate.

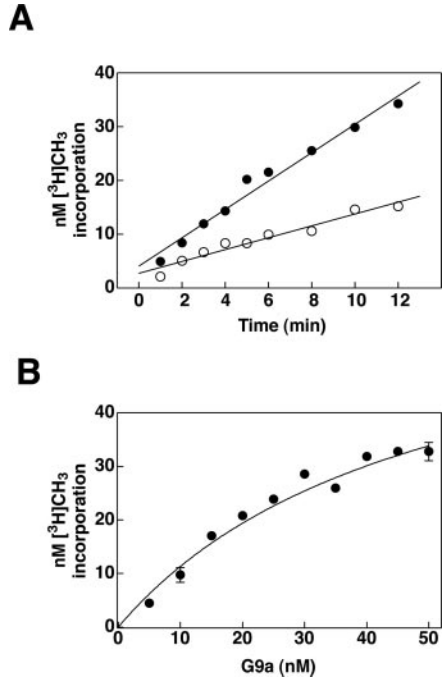

FIG. 5. **Linearity of the methylation reaction catalyzed by recombinant G9a.** *A*, linearity of reaction as a function of time with two different concentrations of AdoMet, 0.5 (*open circle*) and 5 μM (*closed circle*). The reaction contained 2.2 μM K4AK9 substrate, 25 nM full-length G9a along with AdoMet and was incubated at 25 °C. 10 μl of the reaction mixture was spotted in duplicate in P81 at fixed time intervals and processed as described under "Experimental Procedures." The mean values of the radioactive incorporation are plotted along with time. Linear regression of methyl group incorporation is shown for both concentrations of AdoMet. *B*, linearity of the methyl transfer reaction as a function of enzyme concentration. Duplicate reactions of 25 μl containing 2.2 μM K4AK9, 5 μM tritiated AdoMet, and an increasing concentration of recombinant G9a were incubated for 3 min at room temperature and 10 μl of each reaction was spotted and processed. The *filled circles* show nanomolar methyl group incorporation.

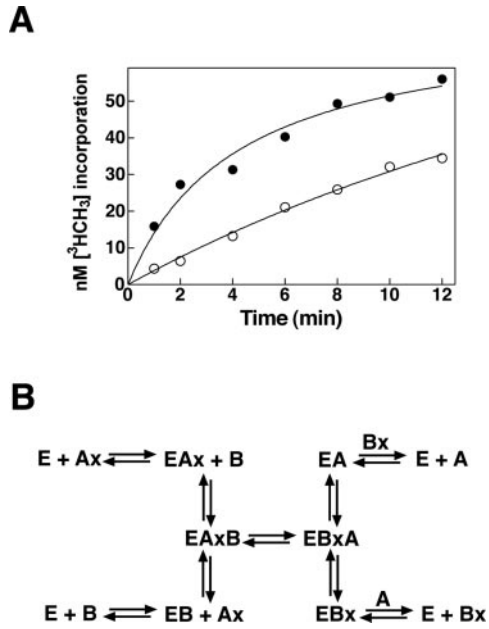

FIG. 6. **Preincubation studies with recombinant G9a and its reaction mechanism.** *A*, preincubation of recombinant G9a, AdoMet, and peptide was performed as described under "Experimental Procedures." Methylation in the presence of preformed G9a-AdoMet binary complex (peptide added second) is shown as a *filled circle*. Similarly preformed G9a-peptide binary complex (AdoMet added second) is shown as a *open circle*. 10 μl of the reaction mixture was spotted in each 2-min time interval and methyl group incorporation was measured. *B*, a scheme of random mechanism catalyzed by recombinant G9a. *E*, G9a; *Ax*, x being methyl group (AdoMet); *B*, unmethylated peptide; *A*, AdoHcy; and *Bx*, methylated peptide, are shown. Binary (EAx, EB, EBx, EA) and ternary (EAxB and EBxA) complexes are shown.

ation. Addition of AdoMet first led to a higher burst of methylation activity in the first 4 min of the reaction followed by a steady gain of methylation, suggesting that G9a-AdoMet is catalytically more potent than the G9a-K4AK9 binary complex in presteady-state reaction conditions (Fig. 6*A*). Higher catalytic potency of the G9a-AdoMet binary complex may be because of the positioning of AdoMet in the active site pocket of the enzyme that may facilitate substrate binding followed by catalysis. The rate of methylation at a given point (after 4 min) between preformed G9a-AdoMet and G9a-K4AK9 complexes remained similar (Fig. 6*A*), suggesting the complexes are catalytically competent. Furthermore, a random order of substrate binding to G9a will result in catalysis. If the reaction mechanism is ordered, only one complex would have been catalytically competent as was observed previously for murine DNA (cytosine-5) methyltransferase I, where the enzyme-AdoMet complex was not competent for catalysis (29). The random order of the reaction will involve the enzyme (*E*) binding to either AdoMet (Ax) or peptide (B) first to make binary complex EAx or EB followed by the second substrate, B or Ax, respectively, to make the ternary EAxB complex. A transition phase for methyl group transfer to B will take place to make the EABx complex. The products will be released in a random way indicating that either the methyl peptide (Bx) release will be followed by enzyme and AdoHcy (A) dissociation, or AdoHcy (A) dissociation followed by enzyme and methyl peptide dissociation. This reaction scheme is described in Fig. 6*B*.

Steady-state Kinetic Properties of Recombinant G9a on Various Peptide and Recombinant Histone H3 Substrates—By studying an enzyme-catalyzed reaction at steady-state one can obtain essential kinetic parameters for a specific enzyme at a set of reaction conditions with a specific substrate. Because G9a can efficiently methylate lysine residues of histone H3 and synthetic peptides representing these sequences (Fig. 2*D*), a series of peptides were used for studying steady-state kinetic properties and reaction mechanisms (Table I). Wild-type peptide was identical to the histone H3 tail because it contains two potential lysine residues (Lys-4 and Lys-9) although only Lys-9 was shown to be methylated. Therefore, to avoid the positional effect of histone methylation in the presence of Lys-4, we mutated K4A and the substrate was termed the K4AK9 peptide. All reactions were carried out for 3 min.

Variable amounts of either bacterial expressed human histone H3 (rH3), Wt-H3, or K4AK9 substrates with saturating amounts

TABLE I
Substrates and methylated peptides used in kinetic analysis of recombinant G9a

The abbreviations used are as follows: biotin (BT), dimethyl-lysine (2-meK), and trimethyl-lysine (3-meK).

Peptide sequence	Peptide name
CARTKQTARKSTGGKAPRK-BT	Wt-H3
ARTKQTARKSTGGKAPRKQL	Wt-H3-nonbiotin
CARTKQTAR(2me-K)STGGKAPRK-BT	Wt-H3-(K9-dime)
CARTAQTARKSTGGY-BT	K4AK9
CARTKQTARASTGGY-BT	K4K9A
CARTAQTARASTGGY-BT	K4A/K9A
CARTAQTAR(2-meK)STGGY-BT	K4AK9-dime
CARTAQTAR(3-meK)STGGY-BT	K4AK9-trime

of AdoMet and a constant amount of recombinant G9a resulted in a hyperbolic curve fitted to Equation 1. Representative Michaelis-Menten plots for velocity as a function of rH3 (Fig. 7*A*), K4AK9 (Fig. 7*B*), and AdoMet concentrations (Fig. 7*C*) are shown. Methylation saturation was obtained above 1.0 μM of the substrate concentration (Table II). The kinetic parameters V_{max} and K_m were obtained after performing a nonlinear regression curve fit. From the V_{max}, k_{cat} was calculated along with the catalytic efficiency of the enzyme. Similar analyses were performed with rH3 substrate and shown in Table II. Furthermore, a series of double reciprocal plots were made at six different AdoMet or six different K4AK9 peptide concentrations. With this analysis the reciprocal of the amount of the tritiated methyl group transferred to the peptide substrate in 1 min by 1 nM enzyme (1/v) was plotted as a function of 1/K4AK9 (Fig. 7*D*) or 1/AdoMet (Fig. 7*E*) in the presence of a fixed co-substrate concentration. For a bireactant enzyme, such as G9a, which uses two substrates and gives rise to two products, the double reciprocal plots usually yield linear regression. The slope and intercepts of these lines may be used for determination of kinetic constants. Slope 1/K4AK9 was plotted against 1/AdoMet to determine K_m^{AdoMet} (data not shown) and was 0.4 ± 0.1 μM. We also determined K_m^{pep} for K4AK9 by plotting slope 1/AdoMet *versus* 1/K4AK9, which was determined to be 1.1 ± 0.1 μM. These values are comparable with the values obtained by the non-linear regression analysis shown in Fig. 5, *A* and *B*, and presented in Table II. Furthermore, the double reciprocal plots with either K4AK9 or AdoMet as variable substrates converged to the left of the *y* axis and above or on the *x* axis, suggesting that the enzyme can methylate in either an ordered or random mechanism. The kinetic constants such as K_m and k_{cat} are derived by non-linear regression and reported in Table II. Furthermore, a series of kinetic parameters with different substrates were determined, compared, and presented in Table II. Human SET9 histone H3-K9 monomethyltransferase turnover number was 3-fold less than G9a on histone H3 substrate (30).

Product Inhibition Studies of Recombinant G9a with AdoHcy and Trimethylated Peptide—Because double reciprocal plots in Fig. 7, *D* and *E*, were not able to distinguish the reaction mechanism of G9a, product inhibition studies were performed. Enzyme inhibitors may act either reversibly or irreversibly. In an enzyme-catalyzed reaction, the most often encountered deviation from hyperbolic kinetics is because of product inhibition. The end product of a reaction has enough affinity for the active site of the enzyme to bind, thus blocking subsequent binding of the substrate molecule (*i.e.* is a competitive inhibitor with respect to one of the substrates). As the concentration of the product increases so does the inhibition effect, thus the observed velocity is lower than expected. Addition of this end product will slow the overall forward rate of the enzymatic reaction and can allow one to distinguish between random and ordered mechanisms. For these studies, one substrate is held constant and the products as well as the other substrates are varied in a concentration range around their Michaelis constant. For an enzyme that requires two substrates, a competitive inhibitor of one of the substrate-binding sites will display the behavior of either a competitive or a mixed inhibitor, depending on the substrate used and its interaction with the enzyme. AdoHcy inhibition with respect to varying AdoMet concentrations yielded double reciprocal plots converging on the *y* axis, thus suggesting that AdoHcy is a competitive inhibitor of AdoMet (Fig. 8*A*). Non-linear fitting of the product *versus* AdoMet concentration gave a series of curves with different $K_{m(app)}$. The K_i value was calculated by plotting $K_{m(app)}$ *versus* AdoHcy (inhibitor) concentration (Fig. 8*C*) and was about 2.3 μM. And when a variable peptide substrate K4AK9 concentration was used along with the fixed AdoMet and AdoHcy products, the double reciprocal plots intersected each other on the left of the *y axis* above the *x* axis, suggesting a mixed inhibition pattern. This mixed inhibition system may be because of the G9a and G9a-AdoHcy binary complex binding to substrate peptide at different affinities. In this case both enzyme-substrate and enzyme-substrate and inhibitor form products at different rates, because both AdoMet and AdoHcy are structurally similar and the G9a-AdoHcy complex after binding to substrate can be catalytically competent if AdoMet replaces AdoHcy. The K_i value was determined by plotting $1/V_{max}$ *versus* the methylated peptide concentration and was about 0.55 μM as shown in Table III.

Because the inhibition pattern with AdoHcy was competitive with AdoMet and mixed with peptide, the mechanism of the reaction may be compulsory ordered or random ordered. Previous reports have suggested both Lys-9 and Lys-27 methylation by G9a (18). Thus the other product of this reaction is trimethylated Lys-9 and Lys-27. To elucidate the reaction mechanism, product inhibition studies were performed with the K4AK9 substrate and trimethylated peptide. In the presence of varied AdoMet substrate concentrations, trimethylated peptide product, and fixed peptide substrate, the family of double reciprocal plots intersected each other on the left of the *y axis* above the *x* axis, suggesting a mixed inhibition pattern (Fig. 8*D*). The K_i for the methylated peptide was 0.66 μM as shown in Fig. 8*F*. However, the family of double reciprocal plots with varied peptide substrate concentrations, trimethylated peptide product, and fixed AdoMet, intersected each other on the *y axis* (Fig. 8*E*). The K_i was calculated by plotting $K_{m(app)}$ values (obtained from non-linear regression of product *versus* K4AK9 concentration curves) *versus* methylated peptide concentration and was about 3.65 μM. The pattern of product inhibition reaction observed for G9a with products of the AdoHcy and trimethylated peptide is summarized in Table II, suggesting that the reaction is a random Bi Bi mechanism.

DISCUSSION

Mammalian histone methyltransferase, G9a, was reported to be responsible for mono- and dimethylation of Lys-9 residues on histone H3 (18, 20), an observation confirmed by the present study using baculovirus expressed recombinant G9a. Furthermore, in an *in vitro* methyl transfer reaction, recombinant G9a was able to transfer three consecutive methyl groups to the ϵ amino group of lysine by both mass spectroscopy analysis as well as sequencing of the enzymatically methylated peptide (Fig. 3). In our assay conditions we were able to trimethylate all of the unmethylated substrate using a highly purified concentrated enzyme, and a well defined peptide substrate. Thus our results demonstrate a direct measurement of enzyme-mediated methylation on the unmethylated substrate. In the G9a knockout embryonic stem cell experiments both Peters *et al.* (20) and Rice *et al.* (31) used an antibody detection method on cell extracts for investigating the substrate specificity of G9a. Us-

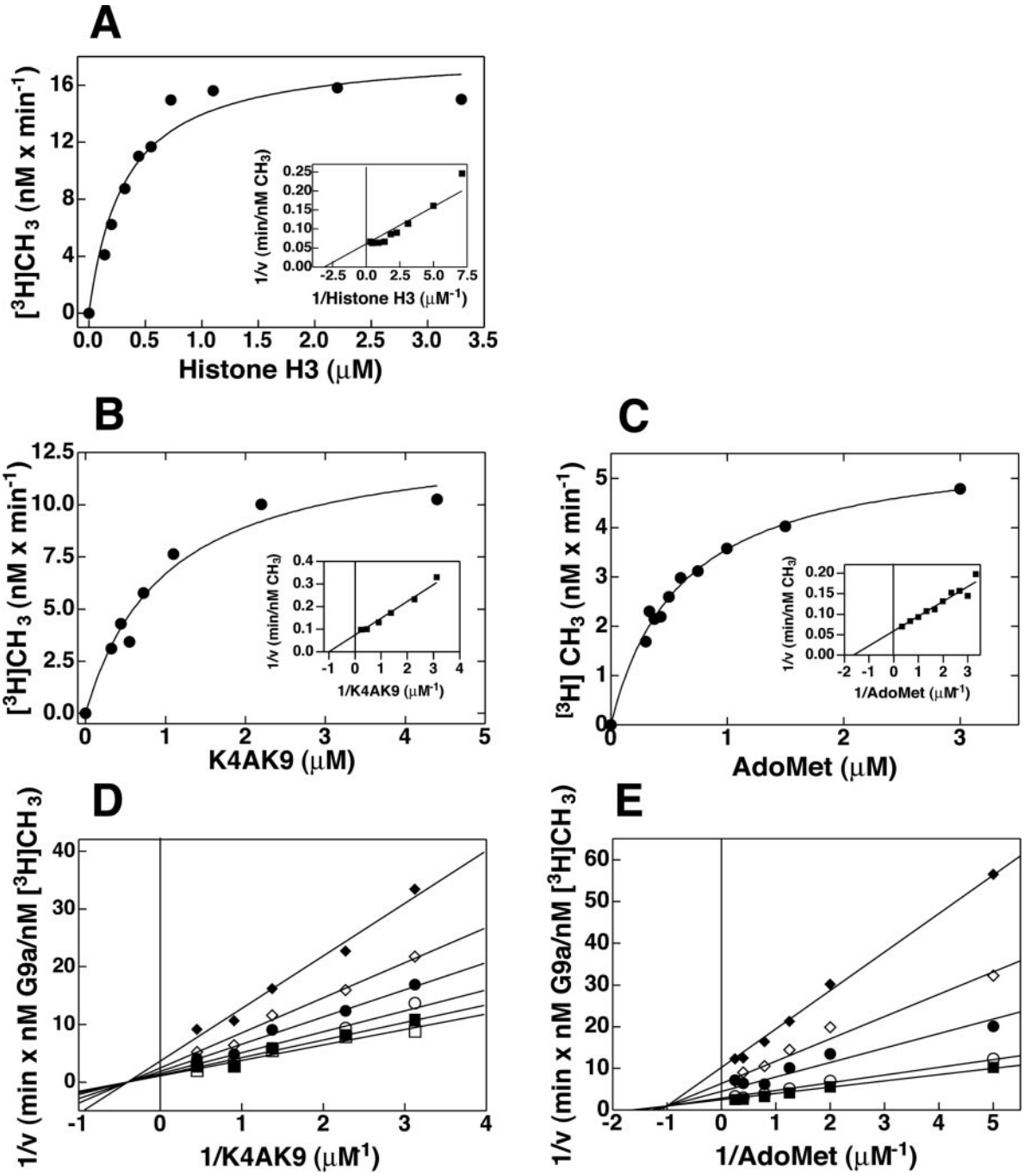

FIG. 7. **Representative substrate-velocity curves and double reciprocal plots of the initial velocity *versus* substrate concentration.** *A*, full-length G9a activity with recombinant full-length histone H3 substrate. Methylation reactions performed with substrate concentrations of 0.14, 0.2, 0.32, 0.44, 0.55, 0.726, 1.1, 2.2, and 3.3 μM and fixed enzyme and AdoMet concentrations of 25 nM and 5 μM, respectively. Product formation is plotted *versus* substrate concentration and non-linear regression was performed for determination of K_m^{H3} values. The *inset* shows the Lineweaver-Burk plot of the substrate velocity. V_{max} and K_m^{H3} were calculated from the substrate velocity plot. *B*, similar substrate velocity curve as that of *A* for variable K4AK9 peptide concentrations (0.32, 0.44, 0.55, 0.726, 1.1, 2.2, 3.3, and 4.4 μM), 25 nM G9a, and 5 μM AdoMet. Product formation is plotted *versus* substrate concentration and non-linear regression was performed for determination of K_m^{pep} values. The Lineweaver-Burk plot of 1/v *versus* 1/s is shown as an *inset*. *C*, another similar substrate velocity curve as that of *B*, for variable AdoMet concentrations (0.333, 0.375, 0.43, 0.5, 0.6, 0.750, 1.0, 1.5, 3.0 μM) with 25 nM G9a and 5 μM K4AK9 peptide. Product formation is plotted *versus* substrate concentration and non-linear regression was performed for determination of K_m^{AdoMet} values. The Lineweaver-Burk plot of the 1/v *versus* 1/s is shown as an *inset*. *D*, double reciprocal plots for fixed AdoMet concentrations of 0.2 (*filled diamond*), 0.5 (*open diamond*), 1.25 (*filled circle*), 1.75 (*open circle*), 2.5 (*filled square*), and 5 μM (*open square*). Linear regression is performed and 1/v is plotted against 1/K4AK9. *E*, double reciprocal plots for fixed peptide concentrations and variable peptide concentrations of 0.32 (*filled diamond*), 0.44 (*open diamond*), 0.726 (*filled circle*), 1.1 (*open circle*), and 2.2 μM (*filled square*). Linear regression is performed and 1/v is plotted against 1/AdoMet.

ing Western blot analysis H3-K9 mono- and dimethylation were severely reduced, leading the authors to conclude that G9a is a mono- or dimethylation-specific enzyme, and Suv39h1, the other H3-K9 methyltransferase is responsible for trimethylation. However, crude *E. coli* lysate expressing G9a was able to methylate dimethylated H3 Lys-9 peptide *in vitro* (31). In the same studies both groups used double knockout Suv39h1 embryonic stem cells to measure H3-K9 trimethylation. Although the majority of H3-K9 trimethylation was reduced, a small but significant amount was detected suggesting that an

TABLE II

Comparison of steady-state kinetic parameters of G9a and other histone H3-K9 methyltransferases enzymes

Peptide nomenclature is presented under "Experimental Procedures." Wt H3 indicates the first 19 amino acids of the amino terminus of histone H3. Wt H3(K9-dm) is the dimethylated Lys-9 peptide. Recombinant bacterial expressed human histone H3 is shown as rH3.

	Substrate	k_{cat}	K_m^{AdoMet}	K_m^{pep}	k_{cat}/K_m^{pep}	Ref.
		h^{-1}	μM	μM	$10^6 \times M^{-1}\ h^{-1}$	
G9afl	Wt-H3	88 ± 4	1.8 ± 0.2	0.9 ± 0.1	98	Present work
G9afl	Wt-H3(K9dm)	12 ± 3		2.3 ± 1.1	5.2	Present work
G9afl	K4AK9	32 ± 2	0.6 ± 0.1	1.0 ± 0.1	32	Present work
G9afl	rH3	46 ± 1	2.65 ± 0.2	0.3 ± 0.05[a]	153[b]	Present work
Human SET9	rH3	14 ± 1	6.0 ± 1.4	5.4 ± 2.1	2.6	Xiao (30)
PeaLSMT[c]	Rubisco	137 ± 4	6.0 ± 1.3	1.4 ± 0.2	98	Trievel (34)
dSU(VAR)3–9	Wild type (1–19)	396	25.9			Eskeland (19)

[a] Represents the value for K_m^{H3}.
[b] Represents the value for k_{cat}/K_m^{H3}.
[c] PeaLSMT is rubisco large subunit methyltransferase.

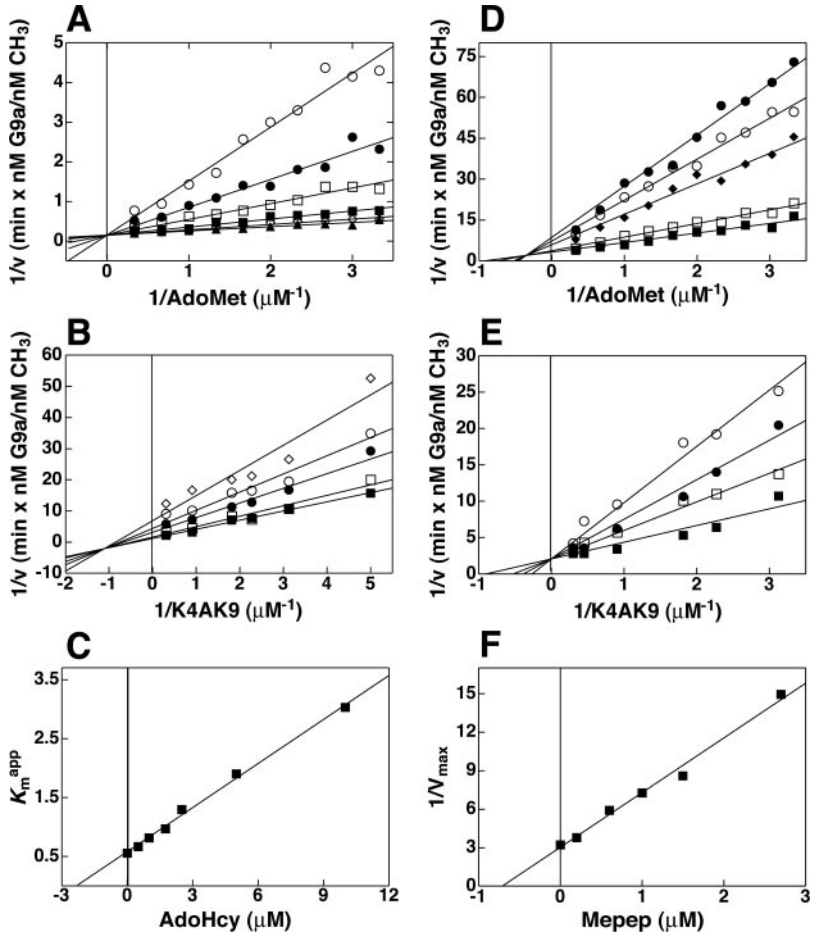

FIG. 8. **Product inhibition analysis of Lys-9 methylation catalyzed by recombinant G9a.** *A*, double reciprocal plot in the presence of a fixed concentration of AdoHcy, 0 (*filled triangle*), 0.5 (*open squares*), 1.0 μM (*filled circles*), 1.75 (*open circles*), and 10 μM (*filled circle*). 1/v is plotted against 1/AdoMet concentration after linear regression. AdoMet concentration was variable (0, 0.3, 0.33, 0.375, 0.429, 0.50, 0.6, 0.75, 1.0, 1.5, and 3.0 μM) in the reaction. *B*, similar to that of *A*, double reciprocal plot in the presence of a fixed concentration of AdoHcy, 0 (*filled squares*), 0.5 (*open diamond*), 1.0 (*filled diamond*), 2.5 (*open square*), 5 (*closed circle*), and 10 μM (*open diamonds*). 1/v is plotted against 1/K4AK9 concentration after linear regression. K4AK9 concentration was variable (0, 0.2, 0.32, 0.44, 0.55, 1.1, and 3.3 μM) in the reaction. *C*, a representative figure depicting deduction of K_i value in AdoMet *versus* AdoHcy competitive inhibition studies. $K_{m(app)}$ obtained by non-linear regression of data set of *A* is plotted against AdoHcy concentration. The K_i value is obtained from the *y* axis intercept. *D*, double reciprocal plot in the presence of a fixed concentration of trimethylated peptide, 0 (*filled square*), 0.2 (*open squares*), 0.6 (*filled diamonds*), 1.0 (*open circles*), and 1.5 μM (*filled circle*). 1/v is plotted against 1/AdoMet concentration after linear regression. AdoMet concentration was variable (0, 0.3, 0.33, 0.375, 0.429, 0.50, 0.6, 0.75, 1.0, 1.5, and 3.0 μM) in the reaction. *E*, similar to that of *D*, double reciprocal plot in the presence of a fixed concentration of trimethylated peptide, 0 (*filled squares*), 2.7 (*open square*), 5.8 (*filled circle*), and 10 μM (*open circle*). 1/v is plotted against 1/K4AK9 concentration after linear regression. K4AK9 concentration was variable (0.32, 0.44, 0.55, 1.1, 2.2, and 3.3 μM) in the reaction. *F*, determination of K_i value from a mixed inhibitor by plotting $1/V_{max}$ (from *D*) against inhibitor (methylated peptide) concentration. The *y* axis intercept gives an estimation of K_i.

enzyme other than Suv39h1 may be involved in maintaining a limited amount of H3-K9 trimethylation. Because the bulk of pericentric heterochromatin is trimethylated by Suv39h1 and a portion of euchromatic genes are silenced by G9a-mediated histone H3 methylation, the small amount of H3-K9 trimethylation observed in Suv39h1 null cells may be maintained by G9a. However, it is possible that G9a may be capable of mono-, di-, and trimethylation *in vitro* but not in *in vivo*. In an *in vivo* situation other regulatory factors may regulate it to be a mono- and dimethylation specific enzyme. In this case,

TABLE III
Product inhibition pattern of recombinant G9a

Peptide used as substrate was K4AK9. Me-peptide is trimethylated Lys-9 and Lys-27 peptides representing the fully methylated end product.

Product	Variable substrate	Fixed substrate	Type of inhibition	Inhibition constant
				μM
AdoHcy	AdoMet	Peptide	Competitive	2.3
AdoHcy	Peptide	AdoMet	Mixed	0.55
Me-peptide	Peptide	AdoMet	Competitive	3.65
Me-peptide	AdoMet	AdoHcy	Mixed	0.66

residual Lys-9 trimethylation observed in Suv39 null cells might be catalyzed by other histone H3-K9 methyltransferases that are yet to be identified.

Recombinant G9a methylates substrate peptides in a processive manner although the turnover number using a Lys-9 dimethyl substrate was seven times slower as compared with Lys-9 methylation of the unmethylated NH_2-terminal tail region of histone H3. Recently, recombinant *Drosophila* Su(var)3–9 was shown to transfer two methyl groups to the NH_2-terminal Lys-9 of histone H3 in a non-processive manner (19). Three other histone methyltransferases such as DIM-5 (32), SET7/9 (30), and peaLSMT (33, 34) have been studied for their ability to transfer methyl groups from cofactor AdoMet to Lys-9 residues, by crystallographic analysis of enzyme substrate complexes. Zhang *et al.* (32) have demonstrated that DIM-5 preferentially trimethylates H3-K9 *in vivo*. This observation was also confirmed *in vitro* where DIM-5 showed rapid methylation kinetics on a synthetic peptide. With an unmodified substrate it produced mono-, di-, and trimethylated species although trimethylated species became dominant after 30 min of the reaction when there were still ample amounts of unmethylated peptides. After careful mass spectroscopy analysis the authors concluded that DIM-5 is capable of converting di- to trimethyl-lysine at a much faster rate than un- to trimethylated lysine. Such an enzyme is classified as processive. The full-length G9a did not prefer converting dimethylated peptides to trimethylated ones as observed by turnover number and catalytic efficiency for dimethylated substrate. Thus the fundamental mechanism of di- to trimethylation of H3-K9 is possibly different between DIM-5 and G9a. However, overnight incubation of recombinant full-length G9a resulted in almost 99% substrate converted to trimethylated lysine, suggesting its potency as a trimethyl-lysine methyltransferase (Fig. 3). This discrepancy is best explained by a ~2.5-fold difference in K_m values of both unmethylated and dimethylated substrate with recombinant full-length G9a, suggesting that dimethylated peptide may have difficulty in binding to the active site as compared with its unmethylated counterpart, thus affecting the catalysis.

To explain the mechanism of trimethylation by G9a, sequence alignment of the active sites of DIM-5 and G9a was performed (data not shown). In DIM-5, the cofactor was surrounded by amino acids Arg-155, Trp-161, Tyr-204, and Arg-238 and was believed to facilitate the movement of the cofactor toward the active site of the enzyme upon substrate peptide binding. The authors have concluded that the movement path of the cofactor would permit exchange of cofactor AdoMet and product AdoHcy, thus driving the reaction in a processive manner without releasing the substrate after each methyl group transfer (32). Such a phenomenon may be operative in G9a because all the above conserved residues are present in the SET domain (Arg-1097, Trp-1103, Tyr-1138, and Arg-1162) of G9a. Furthermore, in human monolysine methyltransferase SET 7/9, the AdoMet surrounding amino acids are Glu-210, Glu-229, Tyr-245, and Arg-293, which are different from both G9a and DIM-5, suggesting that the structural orientation of amino acids in the proximity of AdoMet may influence enzyme activity as observed with DIM-5.

Full-length recombinant G9a methylates Wt-H3 substrate peptide efficiently. The turnover number for full-length G9a was comparable with another SET domain protein methyltransferase LSMT and was at least 6-fold higher than human SET9. In contrast, the K_m^{AdoMet} value for recombinant G9a was much smaller (1.1–2.65 μM) than pea LSMT (6.0 μM), human SET9 (6.0 μM), and *Drosophila* Su(var)3–9 (26 μM). This implies that G9a is capable of methyl transfer reactions even at low cellular concentrations of AdoMet. Mutation of K4A in peptide substrate K4AK9 led to a decrease in both catalytic efficiency and turnover number for full-length G9a (Table II). This suggests that the regulation of Lys-9 methylation may be influenced by modification of Lys-4. Because Lys-4 methylation is mutually exclusive to Lys-9 methylation (35), G9a may have a mechanism to sense the modification status before proceeding with Lys-9 methylation. However, more mechanistic studies need to be performed to elucidate the influence of a Lys-4 modification on Lys-9 methylation.

Overall, the initial velocity data with either constant peptide or AdoMet substrate are consistent with the sequential Bi Bi mechanism (either ordered or random). The linear double reciprocal plots in Fig. 7, *D* and *E*, and preincubation studies demonstrating catalytic competence of the binary complexes (Fig. 6*A*) along with the reaction scheme (Fig. 6*B*) explained the proposed mechanism. We have further confirmed our hypothesis that the substrates follow a random mechanism using product inhibition studies. Several other enzymes, particularly the DNA (cytosine 5) methyltransferases, such as human DNMT1 (36), M.HhaI (37), and M.BamHI (38), also show a random Bi Bi mechanism. It is possible that *in vivo* this mechanism of reaction may be affected by the concentration of AdoMet and other interacting protein partners. Other than the catalytic SET domain, very little is known about the structural and functional aspects of the other regions of G9a. The efficiency of the methyl transfer reaction may also be adjusted with modification of adjacent residues on histone H3, as observed for serine 10 phosphorylation (4). Thus, diverse arrays of post-translational modification of histone H3 may influence its methylation via enzyme substrate binding.

Acknowledgments—We thank Dr. T. Evans for discussion and critical reviews and Dr. Yoichi Shinkai for the murine G9a clone (pZKmG9a). We also thank Dr. Norbert O. Reich for discussion regarding mechanistic aspects of methyltransferases. Technical assistance from Nancy Badger is highly appreciated. We thank Dr. D. G. Comb, New England Biolabs, Inc., for support and encouragement.

REFERENCES

1. Strahl, B. D., and Allis, C. D. (2000) *Nature* **403,** 41–45
2. Brownell, J. E., Zhou, J., Ranalli, T., Kobayashi, R., Edmondson, D. G., Roth, S. Y., and Allis, C. D. (1996) *Cell* **84,** 843–851
3. Borun, T. W., Pearson, D., and Paik, W. K. (1972) *J. Biol. Chem.* **247,** 4288–4298
4. Rea, S., Eisenhaber, F., O'Carroll, D., Strahl, B. D., Sun, Z. W., Schmid, M., Opravil, S., Mechtler, K., Ponting, C. P., Allis, C. D., and Jenuwein, T. (2000) *Nature* **406,** 593–599
5. Noma, K., Allis, C. D., and Grewal, S. I. (2001) *Science* **293,** 1150–1155
6. Heard, E. (2004) *Curr. Opin. Cell Biol.* **16,** 247–255
7. Kondo, Y., Shen, L., Yan, P. S., Huang, T. H., and Issa, J. P. (2004) *Proc. Natl. Acad. Sci. U. S. A.* **101,** 7398–7403
8. Tamaru, H., and Selker, E. U. (2001) *Nature* **414,** 277–283
9. Jackson, J. P., Lindroth, A. M., Cao, X., and Jacobsen, S. E. (2002) *Nature* **416,** 556–560
10. Soppe, W. J., Jasencakova, Z., Houben, A., Kakutani, T., Meister, A., Huang, M. S., Jacobsen, S. E., Schubert, I., and Fransz, P. F. (2002) *EMBO J.* **21,** 6549–6559
11. Tariq, M., Saze, H., Probst, A. V., Lichota, J., Habu, Y., and Paszkowski J. (2003) *Proc. Natl. Acad. Sci. U. S. A.* **100,** 8823–8827
12. Lehnertz, B., Ueda, Y., Derijck, A. A., Braunschweig, U., Perez-Burgos, L., Kubicek, S., Chen, T., Li, E., Jenuwein, T., and Peters, A. H. (2003) *Curr. Biol.* **13,** 1192–1200

13. Bachman, K. E., Park, B. H., Rhee, I., Rajagopalan, H., Herman, J. G., Baylin, S. B., Kinzler, K. W., and Vogelstein, B. (2003) *Cancer Cell* **3,** 89–95
14. Nakayama, J., Rice, J. C., Strahl, B. D., Allis, C. D., and Grewal, S. I. (2001) *Science* **292,** 110–113
15. Tschiersch, B., Hofmann, A., Krauss, V., Dorn, R., Korge, G., and Reuter, G. (1994) *EMBO J.* **13,** 3822–3831
16. Schultz, D. C., Ayyanathan, K., Negorev, D., Maul, G. G., and Rauscher, F. J. (2002) *Genes Dev.* **16,** 919–932
17. Yang, L., Xia, L., Wu, D. Y., Wang, H., Chansky, H. A., Schubach, W. H., Hickstein, D. D., and Zhang, Y. (2002) *Oncogene* **21,** 148–152
18. Tachibana, M., Sugimoto, K., Fukushima, T., and Shinkai, Y. (2001) *J. Biol. Chem.* **276,** 25309–25317
19. Eskeland, R., Czermin, B., Boeke, J., Bonaldi, T., Regula, J. T., and Imhof, A. (2004) *Biochemistry* **43,** 3740–3749
20. Peters, A. H., Kubicek, S., Mechtler, K., O'Sullivan, R. J., Derijck, A. A., Perez-Burgos, L., Kohlmaier, A., Opravil, S., Tachibana, M., Shinkai, Y., Martens, J. H., and Jenuwein T. (2003) *Mol. Cell.* **12,** 1577–1589
21. Xin, Z., Tachibana, M., Guggiari, M., Heard, E., Shinkai, Y., and Wagstaff, J. (2003) *J. Biol. Chem.*, **278,** 14996–15000
22. Yeates, T. O. (2002) *Cell* **111,** 5–7
23. Pradhan, S., Talbot, D., Sha, M., Benner, J., Hornstra, L., Li, E., Jaenisch, R., and Roberts, R. J. (1997) *Nucleic Acids Res.* **25,** 4666–4673
24. O'Reilly, D. R., Miller, L. K., and Luckow, V. A. (1992) in *Baculovirus Expression Vectors: A Laboratory Manual*, pp. 124–127, W. H. Freeman, New York
25. Matsudaira, P. (1987) *J. Biol. Chem.* **262,** 10035–10038
26. Waite-Rees, P. A., Keating, C. J., Moran, L. S., Slatko, B. E., Hornstra, L. J., and Benner, J. S. (1992) *J. Bacteriol.* **173,** 5207–5219
27. Segal, I. H. (1975) *Enzyme Kinetics: Behavior and Analysis of Rapid Equilibrium and Steady-state Enzyme Systems*, John Wiley and Sons, Inc., New York.
28. Crankshaw, M. W., and Grant, G. A. (1993) in *Protein Sequence Analysis*, First Ed., pp. 1–38, Association of Biomolecular Resource Facilities, Bethesda, MD
29. Flynn, J., and Reich, N. O. (1998) *Biochemistry* **37,** 15162–15169
30. Xiao, B., Jing, C., Wilson, J. R., Walker, P. A., Vasisht, N., Kelly, G., Howell, S., Taylor, I. A., Blackburn, G. M., and Gamblin, S. J. (2003) *Nature* **421,** 652–656
31. Rice, J. C., Briggs, S. D., Ueberheide, B., Barber, C. M., Shabanowitz, J., Hunt, D. F., Shinkai, Y., and Allis, C. D. (2003) *Mol. Cell* **12,** 1591–1598
32. Zhang, X., Yang, Z., Khan, S. I., Horton, J. R., Tamaru, H., Selker, E. U., and Cheng, X. (2003) *Mol. Cell* **12,** 177–185
33. Trievel, R. C., Flynn, E. M., Houtz, R. L., and Hurley, J. H. (2003) *Nat. Struct. Biol.* **10,** 545–552
34. Trievel, R. C., Beach, B. M., Dirk, L. M., Houtz, R. L., and Hurley, J. H. (2002) *Cell* **111,** 91–103
35. Wang, H., Cao, R., Xia, L., Erdjument-Bromage, H., Borchers, C., Tempst, P., and Zhang, Y. (2001) *Mol. Cell* **8,** 1207–1217
36. Bacolla, A., Pradhan, S., Roberts, R. J., and Wells, R. D. (1999) *J. Biol. Chem.* **274,** 33011–33019
37. Vilkaitis, G., Merkiene, E., Serva, S., Weinhold, E., and Klimasauskas, S. (2001) *J. Biol. Chem.* **276,** 20924–20934
38. Malygin, E. G., Zinoviev, V. V., Evdokimov, A. A., Lindstrom, W. M., Jr., Reich, N. O., and Hattman, S. (2003) *J. Biol. Chem.* **278,** 15713–15719